ECS Journal of Solid State Science and Technology

High throughput Germanium Homoepitaxy using $GeCl_4$ in an APCVD Batch Reactor

To cite this article: Ella Susann Supik *et al* 2025 *ECS J. Solid State Sci. Technol.* **14** 095002

View the article online for updates and enhancements.

You may also like

- Green-Synthesized Activated Carbon and CNT-Wrapped $NiFePO_4$ Nanocomposite for Advanced Energy Storage and Hydrogen Evolution Applications
Muhammad Ali Hamza Shahbaz, Areej S. Alqarni, Abhinav Kumar et al.
- A Review of Zinc Stannate (Zn_2SnO_4) Resistive Gas Sensors
R. Dhahri, M. Hjiri, Hasan B. Albargi et al.
- Fabrication and Piezoelectric Output Characterization of MXene-Modified Poly(vinylidene fluoride-co-trifluoroethylene) Composite Films
Jiahao Huang, Jun Luo and Yuanyu Wang

ECC-Opto-10 Optical Battery Test Cell:
Visualize the Processes Inside Your Battery!

EL-CELL®
electrochemical test equipment

- Battery Test Cell for Optical Characterization
Designed for light microscopy, Raman spectroscopy and XRD.
- Optimized, Low Profile Cell Design (Device Height 21.5 mm)
Low cell height for high compatibility, fits on standard samples stages.
- High Cycling Stability and Easy Handling
Dedicated sample holders for different electrode arrangements included!
- Cell Lids with Different Openings and Window Materials Available

Scan me!

Contact us:
+49 40 79012-734
sales@el-cell.com
www.el-cell.com

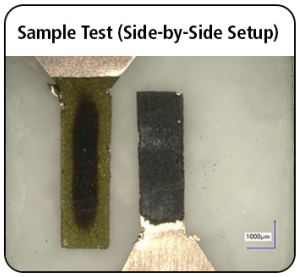

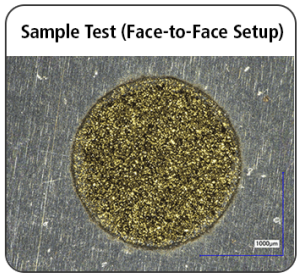

ECS Journal of Solid State Science and Technology, 2025 **14** 095002

High throughput Germanium Homoepitaxy using $GeCl_4$ in an APCVD Batch Reactor

Ella Susann Supik,[1,2,z] Waldemar Schreiber,[2] Andy Wagenfeldt,[2] Jinyoun Cho,[3] Kristof Dessein,[3] Zamin Mamiyev,[4] Christoph Tegenkamp,[4] Charlotte Weiss,[2] and Andreas Walter Bett[1,2]

[1] *University of Freiburg, Physics Institute, Freiburg, Germany*
[2] *Fraunhofer Institute for Solar Energy Systems ISE, Freiburg, Germany*
[3] *Umicore, Electro-Optic Materials, Olen, Belgium*
[4] *University of Technology Chemnitz, Physics Institute, Chemnitz, Germany*

To meet the rising demand for germanium, a critical raw material commonly used as substrates for highly efficient III−V solar cells, innovative, sustainable and cost-effective substrate alternatives, such as engineered germanium substrates and germanium on silicon virtual substrates, are currently under development. In this study, we developed a high throughput homoepitaxial germanium deposition process that can be applied to both substrate alternatives. We successfully deposited 10 μm thick, high-quality germanium epilayers at an elevated growth rate and high molar yield without compromising quality utilizing a batch-type atmospheric pressure chemical vapor deposition (APCVD) reactor in a $GeCl_4$–H_2 system. Under optimal deposition conditions at 750 °C with a $GeCl_4/H_2$ ratio of 1.11×10^{-2}, we achieved a significant growth rate of 0.37 μm min^{-1} and a molar yield of 36%. Characterization of the crystalline structure and surface morphology confirmed that the epilayers exhibit high crystalline quality, comparable to bulk Czochralski wafers, affirming their suitability as substrates for highly efficient III−V solar cells.
 [DOI: 10.1149/2162-8777/ae08e4]

Manuscript submitted June 14, 2025; revised manuscript received September 5, 2025. Published September 30, 2025.

Germanium is in high demand for various applications including infrared detectors, optical fibres, polymer catalysis and as substrates for highly efficient III−V solar cell space applications.[1,2] By 2050, germanium consumption is projected to double compared to 2019, with solar cells anticipated to be a primary driver, showing an expected annual growth rate of 7%, as the use of highly efficient III−V solar cells is expected to expand from space photovoltaics to terrestrial photovoltaics.[2] For III−V solar cell applications, germanium as substrates are particularly of interest due to the high carrier mobility, the enabled absorption of light in the infrared range and the compatibility of the germanium lattice parameter with III−V semiconductor materials.[1,3] However, due to the high density of germanium, the substrate contributes to up to 90% of the weight of the solar cell.[4] The most significant drawback is that germanium is a critical raw material[5] due to its limited absolute availability and supply risk,[6] leading to high costs for all applications fabricated on Czochralski (Cz) germanium bulk substrates.

Innovative, economic and sustainable technological advancements in germanium substrate design are necessary to meet the market demand in a sustainable way. Two main routes to reduce the amount of germanium consumed per device are the focus of ongoing research to address this problem: (1) virtual substrates, where germanium is epitaxially deposited on Si bulk substrates by either a two-step approach[7] or the use of SiGe-buffer layers up to a Ge content of 100%,[8] enabling the integration of III−V semiconductors on Si substrates, and more recently (2) engineered germanium substrates such as the Ge-on-Nothing (GEON) approach,[9] the Kerfless-wafer approach,[10,11] the Porous germanium Efficient Epitaxial Layer Release PEELER process,[4] all based on the idea of liftable epitaxial layers[12–14] to enable the reuse of germanium bulk substrates.[15]

Both routes are more sustainable, reduce the substrate weight and the cost by consuming less germanium and both routes share a common requirement: a high-quality germanium epitaxial layer that is scalable for larger batch sizes and ready for III−V deposition in MOVPE reactors. To ensure reliable nucleation of the III−V epitaxy, the substrate must have a 6° miscut towards [111] and a surface roughness below 1 nm.[1,16–18] This study focuses on the development of a thick (>10 μm) homoepitaxial deposition process for germanium with high growth rates, which can later be transferred to either of the two aforementioned routes or substrate alternatives. The resulting epilayer increases the mechanical stability required during processing and, when appropriately doped, can also function as an active absorber in the final III−V solar cell device.

Homoepitaxial deposition of germanium in an atmospheric pressure chemical vapor deposition (APCVD) $GeCl_4$–H_2 system was primarily investigated in the latter half of the 20th century achieving high growth rates up to 0.3 μm min^{-1}, on small samples (1 to 2 inches) in rather simplistic reactor setups.[19,20] Later, the direct heteroepitaxial deposition of Ge-on-Si substrates using more advanced single wafer systems such as reduced pressure CVD (RPCVD) or even plasma enhanced CVD (PECVD) gained in interest. Only recently homoepitaxial deposition of germanium has resurged with the introduction of new engineered germanium substrates.[21]

In contrast to RPCVD and PECVD, APCVD, offers several advantages, including lower equipment costs due to the absence of extensive vacuum pump systems, particularly in scaled-up batch systems.[22–24] Additionally, APCVD enables higher growth rates in the mass-transport-limited growth regime, where reaction kinetics are improved by elevated temperatures and homogeneous layer to layer growth is facilitated by the high pressures reducing the surface diffusivity.[24] An APCVD batch type reactor is therefore assumed to be a suitable candidate to achieve a high yield and fast epitaxial deposition of germanium in the mass-transport-limited growth regime, potentially enabling commercial applications.

Germane (GeH_4) and germanium tetrachloride ($GeCl_4$) are the most prominent precursors for germanium epitaxy.[25] While research has historically focused more on the epitaxial deposition using GeH_4,[26,27] a comparative study by Park et al. found that $GeCl_4$ offers slightly higher growth rates and produces smoother layers, particularly at high temperatures in the mass-transport-limited growth regime.[28] The presence of HCl, a byproduct of the pyrolysis deposition reaction of $GeCl_4$ prevents the parasitic deposition on the chamber walls, allowing a thicker deposition of epitaxial layers. $GeCl_4$ has demonstrated its effectiveness as a precursor for high temperature homoepitaxy of thick germanium epilayers (>10 μm),

[z] E-mail: ella.susann.supik@fraunhofer.ise.de

yielding smooth layers with good growth rates and minimal parasitic deposition on chamber walls.[9,29] Additionally, a key advantage of $GeCl_4$ is its greater sustainability and cost-effectiveness compared to GeH_4, as it is an intermediate product in the germanium purification process, eliminating the need for additional synthesis steps.[6]

The aim of this study is to develop a homoepitaxial germanium deposition process in a batch-type APCVD reactor, in a $GeCl_4$–H_2 based environment, to produce 10 μm thick high-quality germanium epilayers at a high growth rate and high yield, without compromising the epilayer quality. First the process parameters to achieve high growth rates are determined, then the quality of the produced epilayers at the selected conditions is analyzed.

Experimental

The homoepitaxial deposition process of germanium was developed in the atmospheric pressure chemical vapor deposition (APCVD) reactor "PE 2061S" purchased from LPE (today ASM), usually used for Si epitaxy for microelectronic devices. It is a barrel-type reactor which can hold up to 14 × 6 inch wafers. A sketch of the essential features of the setup is depicted in Fig. 1. The SiC coated graphite susceptor is inductively heated by the coil surrounding the quartz bell-jar. Hence, the samples are heated from the backside. This hinders parasitic deposition on the bell-jar.

To avoid cross-contamination from previous processes, the susceptor is etched back with gaseous HCl and coated with polysilicon using Trichlorosilane ($SiHCl_3$) prior to each process. The loading area is positioned in a gray-room environment to reduce introduction of contaminating particles. It is important to note that the samples are thereby inevitably exposed to oxygen during mounting. An in situ hydrogen prebake above 700 °C of approximately 20 min is done prior to germanium epitaxy to eliminate the GeO_2-passivation layer[25] while simultaneously assuring a stable process temperature for deposition.

Highly p-type gallium doped 6 inch germanium Czochralski (Cz) wafers were provided by Umicore® as epiready substrates. The substrates are dislocation-free, have a (100)-orientation with a 6°-offcut towards the nearest [111]-direction and a thickness of ~225 μm.

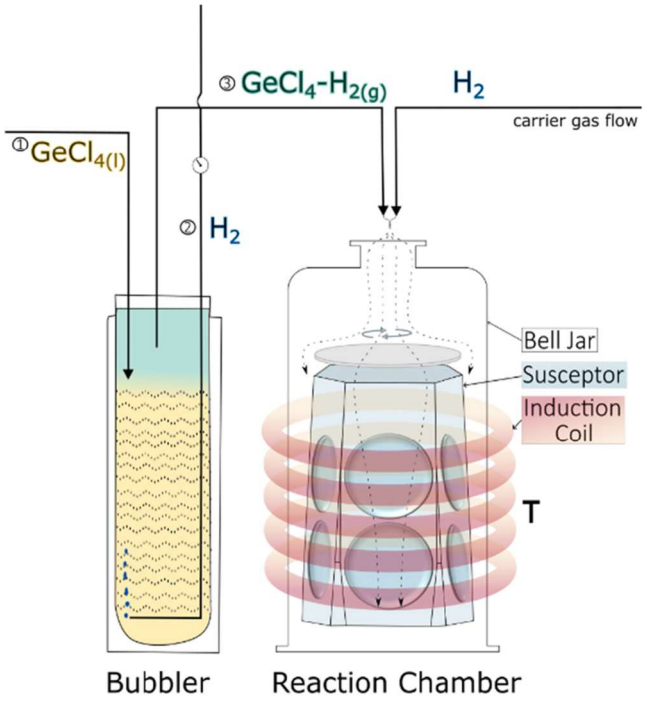

Figure 1. A schematic representation of the APCVD reactor setup used. The left section illustrates the bubbler containing liquid $GeCl_4$ (yellow ①), with H_2 (blue ②) introduced from the bottom. The $GeCl_4$-H_2 vapor mix (green ③) forms at the top of the bubbler. In the reaction chamber (right), samples are heated from the backside by the susceptor, which is heated by induction coils (red) surrounding the bell jar.

High grade germanium tetrachloride ($GeCl_4$), provided by Umicore® and hydrogen (H_2), used as the precursor and carrier gas respectively, are introduced into the chamber from the top. A probable path of the gas flow suggested by the geometric design of the setup is indicated in Fig. 1, the impact of temperature and susceptor rotation on the distribution and convection of the gas stream during processing is not considered here. The $GeCl_4$ source gas passes through a hydrogen bubbler system which is kept at a constant temperature and bubbler-pressure assuring that the vapor pressure is kept constant resulting in a constant $GeCl_4$–H_2 gas mix from the bubbler for all processes.

To determine the optimal process parameters to produce 10 μm thick undoped high-quality germanium epitaxial layers (epilayers) at a high growth rate and yield, the influence of the $GeCl_4/H_2$ ratio was varied in a range of 0.36×10^{-2} to 1.11×10^{-2} by adjusting the carrier gas hydrogen flow and the process temperature is varied in a range of 690 °C to 850 °C. Other process parameters such as the 30 min deposition time, the rotation speed of 6 rotations per minute (rpm), the vapor pressure and flow of $GeCl_4$–H_2 mix from the source bubbler and the prebake-step under hydrogen atmosphere remained constant for all experiments.

The achieved average epilayer thickness for each process was determined by gravimetry, weighing the wafers prior to each process, and after. A 1 μm germanium epilayer on a 6 inch wafer substrate corresponds to 0.1 g of weight difference. From this the growth rate, the molar yield and the gas consumption could be calculated. The molar yield is calculated by taking the total susceptor area (~7000 cm^2 including the area of the susceptor pockets) into account, assuming the thickness on the heated susceptor area is homogeneous and equal to the thickness deposited on the substrates. Hence, 100% yield would mean that all germanium atoms introduced into the chamber are deposited on the susceptor and samples, and nothing is discarded into the exhaust.

The epilayer thickness determined by gravimetry was confirmed by looking at cross sections at the scanning electron microscope (SEM, Hitachi SU-70), where a clear interface between highly p-type doped substrate and undoped epilayer could be seen using a secondary electron detector which is sensitive to doping differences. The thickness homogeneity over the wafer area was determined by thickness mappings by the means of a non-contact surface measurement tool (CT250T by cyberTECHNOLOGIES) and evaluated with the Scan CT 8 software. For gravimetry as well as for thickness mappings, the measurement of the substrate before epitaxy is required. This was done for a limited selection of wafers to reduce their exposure to oxygen and to decrease the introduction of particles and contaminants into the reactor.

For clarity, four categories of thickness homogeneity are defined. The wafer-to-wafer or epilayer-to-epilayer homogeneity compares the thickness of wafers from the same batch, including different susceptor positions (top and bottom pockets). The within-wafer or within-epilayer homogeneity describes the uniformity across a single wafer. Hereby wafer thickness includes both substrate and epilayer, while epilayer homogeneity excludes the substrate contribution.

All roughness values are given by the root-mean-square roughness (RMS), measured by atomic force microscopy (AFM, Park Systems, XE-100) on 5 μm × 5 μm areas at the center of the wafer. The average roughness values correlated to specific experimental parameters are calculated for at least two wafers of each experiment.

The crystalline quality of the epilayers was evaluated by rocking curves of the (400) Ge reflection by the means of high-resolution X-ray diffraction (HR-XRD) (Panalytical X'Pert MRD) in a triple axis configuration using the Copper K_α wavelength. To analyze the surface quality, a spot profile analysing low energy electron diffraction (SPA-LEED) system[30] was used. The experiments were executed in a vacuum system at a base pressure of 5×10^{-9} Pa. An annealing step at 850 °C for 5 min was done to remove the native

oxide prior to the measurement. The diffraction pattern was produced at room temperature using an electron energy of 160 eV.

The structural defect density was determined by counting of the etch features under the optical microscope (nSpec LS-300 by Nanotronics) after defect selective etching (DSE). For this, the sample was subjected to a defect selective etchant Jeita-2[31] consisting of HF(50%), HNO_3 (69%), CH_3COOH (99.9%) and H_2O in the ratio 1:14.5:5.80:5.80 and 0.019 g l^{-1} potassium-iodide[a]. This defect etchant was developed for silicon, nevertheless a similar effectiveness of the etchant is expected for Jeita-2[31] on germanium, as a similar etchant of the same constituents but with I_2 instead of KI as an activating species has been reported to work well on Ge-on-Si samples in literature.[29,33] The DSE process and defect analysis used to determine stacking fault and dislocation densities in germanium are still under development in our group, therefore understanding the classification of etch features is still ongoing. So far, only an upper limit of the dislocation density can be given, as each etch feature is currently counted as a dislocation.

The quality of the epilayers is evaluated by direct comparison with the epiready substrates characterized using the techniques described above.

Results

Process parameters achieving fast growth rates and high yield in an APCVD reactor could be determined in this work. First, the influence of the hydrogen flow, linear gas stream velocity and deposition temperature on the epilayer growth rate was investigated. Fig. 2 shows the resulting correlations. Focusing on the effect of the $GeCl_4/H_2$-ratio, it becomes apparent that an increased hydrogen flow decreases the growth rate. Changing the $GeCl_4/H_2$-ratio from 1.11×10^{-2} to 0.36×10^{-2} at 755 °C (orange diamond) decreases the growth rate from 0.37 μm min^{-1} to 0.24 μm min^{-1}. The observed change in growth rate with varying $GeCl_4/H_2$-ratio reflects the effect of the total mass flow, as keeping the $GeCl_4$ flow constant while changing the hydrogen flow alters the relative $GeCl_4$ fraction and thus the overall mass flow. By keeping a constant flow of $GeCl_4$-H_2 mix coming from the bubbler and only variating the diluting hydrogen carrier gas flow, not only the ratio of $GeCl_4/H_2$-ratio, but also the linear gas stream velocity, defined as the total flow in cm^3 min^{-1} divided by the cross-sectional area of the gas chamber changes. The linear gas stream velocity and $GeCl_4/H_2$-ratio in this set up are therefore directly linked. It should be noted that the gas stream velocity is viewed as a reference point only, as the flow perturbs due to rotation of the susceptor at 6 rpm and convection of gas in the chamber, resulting in a non-linear gas stream velocity throughout the chamber.

The correlation of deposition temperature in a range of 690 °C up to 850 °C and growth rate was investigated for an $GeCl_4/H_2$-ratio of 1.11×10^{-2}. With increasing temperature, the growth rate increases, but it is apparent that temperature has a much smaller impact on the growth rate than the hydrogen flow. An increase of temperature by 160 °C increases the growth rate by 0.05 μm min^{-1} (not linear), whereas an increase of the growth rate by 0.1 μm min^{-1}, is achieved by decreasing the hydrogen flow.

For better understanding, the most important experiments are categorized according to their temperature and hydrogen flow in Table I. The standard deviation of the thickness, growth rate and molar yield in Table I represent the wafer-to-wafer variation of one batch. The wafer-to-wafer thickness homogeneity is within the same range measured for a batch of epiready germanium Cz substrates. For experiment H_2-low the deposition time was doubled to check if the growth rate remains constant even for longer deposition times, this proved to be true.

All wafers with epitaxially grown germanium produced in this series of experiments have a visually, reflective, mirror-like surface, suggesting a good surface topography. A maximum growth rate of up to 0.39 μm min^{-1} and a yield of 38% could be achieved, in experiment

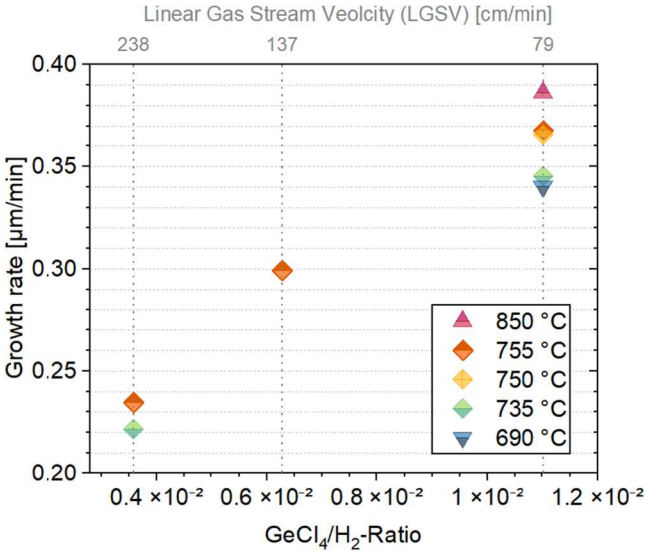

Figure 2. Influence of $GeCl_4/H_2$-ratio and temperature on the growth rate of the germanium epilayers. The top axis shows the corresponding linear gas stream velocity (LGSV) [cm min^{-1}].

T-high, with a process temperature of 850 °C and a low hydrogen flow. The thermal expansion[b] of germanium at 850 °C constitutes to a lateral extension of the wafer by approximately 1 mm, which is enough to reach the edge of the susceptor pockets during heat up and deposition. During cool down, the wafer is reduced to its original size. As a result, the wafers were visibly strained and bowed, which makes them unsuitable for further processing. Hence, the growth parameters of T-high are classified as unsuitable despite the high achievable yield and growth rate. Lowering the process temperature to 750 °C, as in experiment T-med, the lateral extension is reduced and no contact to the pocket rims occurs. As a result, no bowing of the wafers and apparent strain-artefacts were observed.

Experimental parameters of T-med are therefore selected as the most promising growth conditions, achieving a molar yield and growth rate of 36% and 0.37 μm min^{-1}. Germanium epilayers with an average thickness of 11.0 μm could be achieved for sample group T-med within 30 min deposition time. The standard deviation of 0.3 μm of the epilayer thickness reveals a good wafer-to-wafer homogeneity across the whole batch.

The large bell volume (~113 l) and vertical setup of the reaction chamber calls for a high carrier gas flow, and a high gas velocity to assure homogeneous gas flow and gas distribution from top to bottom depositing epilayers with a homogenous thickness on all samples. Gas distribution is improved by rotation of the susceptor throughout the processes. Nevertheless, in all experiments, we observed a higher growth rate in the bottom pocket compared to wafers in the top pocket. The maximum growth rates in Table I correspond to a bottom-pocket wafer, while the minimum corresponds to a top-pocket wafer. Based on the mean deposited thickness, T-med shows the best epilayer-to-epilayer homogeneity, with a relative top-to-bottom pocket epilayer thickness variation of 3.7% this is within the range measured for the epiready Cz germanium substrates. The thickness mappings confirm the higher deposition rate on substrates mounted in the bottom pocket of the susceptor.

The thickness homogeneity within a wafer measured in the thickness mappings was comparable for all experiments listed in Table I, no influence of the gas flow, or temperature could be identified. The thickness mapping of a bottom pocket sample of H_2-med shown in Fig. 3, showed the features discussed in the following paragraph in a more apparent way, and was thus selected here. A microscopic ripple-like surface morphology along the wafer diagonal with a height difference less than 1 μm is apparent. This

[a]The potassium-iodide (KI) is instantly oxidized by HNO_3 to Iodine (I_2).[32]

[b]Lateral thermal expansion calculated as $\Delta l = \alpha l_o \Delta T$, with $\alpha = 7.47 \times 10^{-6}$ K^{-1}.[34]

Table I. Categorization of experiments listing the prominent growth parameters. The table provides the epilayer thickness determined by gravimetry, the calculated growth rate, and molar yield, along with the standard deviation of these values, where all weighed samples are taken into account, thereby representing the wafer-to-wafer homogeneity of a batch.

Sample Group	Ratio $GeCl_4/H_2$	Flow H_2	T °C	Growth rate			Molar yield %	Thickness μm
				μm min^{-1}	max	min		
H_2-high	0.36×10^{-2}	high	755	0.24 ± 0.02	0.25	0.22	23 ± 2	7.0 ± 0.5
H_2-med	0.63×10^{-2}	Med.	755	0.30 ± 0.01	0.31	0.29	29 ± 1	9.0 ± 0.4
H_2-low	1.11×10^{-2}	low	755	0.37 ± 0.02	0.40	0.31	36 ± 2	22.0 ± 1.2
T-high	1.11×10^{-2}	low	850	0.39 ± 0.04	0.50	0.34	38 ± 4	12.0 ± 1.4
T-med	1.11×10^{-2}	low	750	0.37 ± 0.01	0.38	0.35	36 ± 1	11.0 ± 0.3
T-low	1.11×10^{-2}	low	690	0.34 ± 0.01	0.35	0.33	33 ± 1	10.2 ± 0.3

surface morphology originates from the template surface morphology and is therefore replicated by the epilayer. The ripples are not visible by eye or under the microscope. Furthermore, all substrates before epitaxial deposition show a wedge-like thinning from the bottom left to the top right, which coincides with the microscopic surface morphology. Both features are assumed to be a remaining feature of sawing 6°−offcut wafers from the Cz ingot. The total thickness variation (TTV) of 2.5% for the wafer (including substrate and epilayer), as determined from the thickness map in Fig. 3, is predominantly ascribed to the ripple-like feature of the template substrate.

The extracted epilayer thickness is shown in the horizontal (P1) and vertical (P2) profiles respectively. The thickness of the deposited epilayer decreases from 12 μm at the top to 9 μm towards the bottom of the wafer. Since this sample is a bottom pocket wafer, the observed epilayer thinning is inconsistent with the overall trend, where bottom pocket wafers generally have a thicker epilayer than top pocket wafers. P1 in Fig. 3 shows increased deposition towards the horizontal edges of the wafer; however, in the central region of the wafer (x = 20–120 mm), the epilayer thickness is more homogeneous, with an average of 9.7 ± 0.4 μm. Comparing the thickness profiles of the substrate-only to the epilayer-thickness, it is apparent that increased deposition occurs at thinner areas of the substrate, this leads to a homogenization of the total wafer thickness, reducing the wedge-like thinning of the substrate and resulting in a reduced relative TTV after epitaxy. The average epilayer thickness

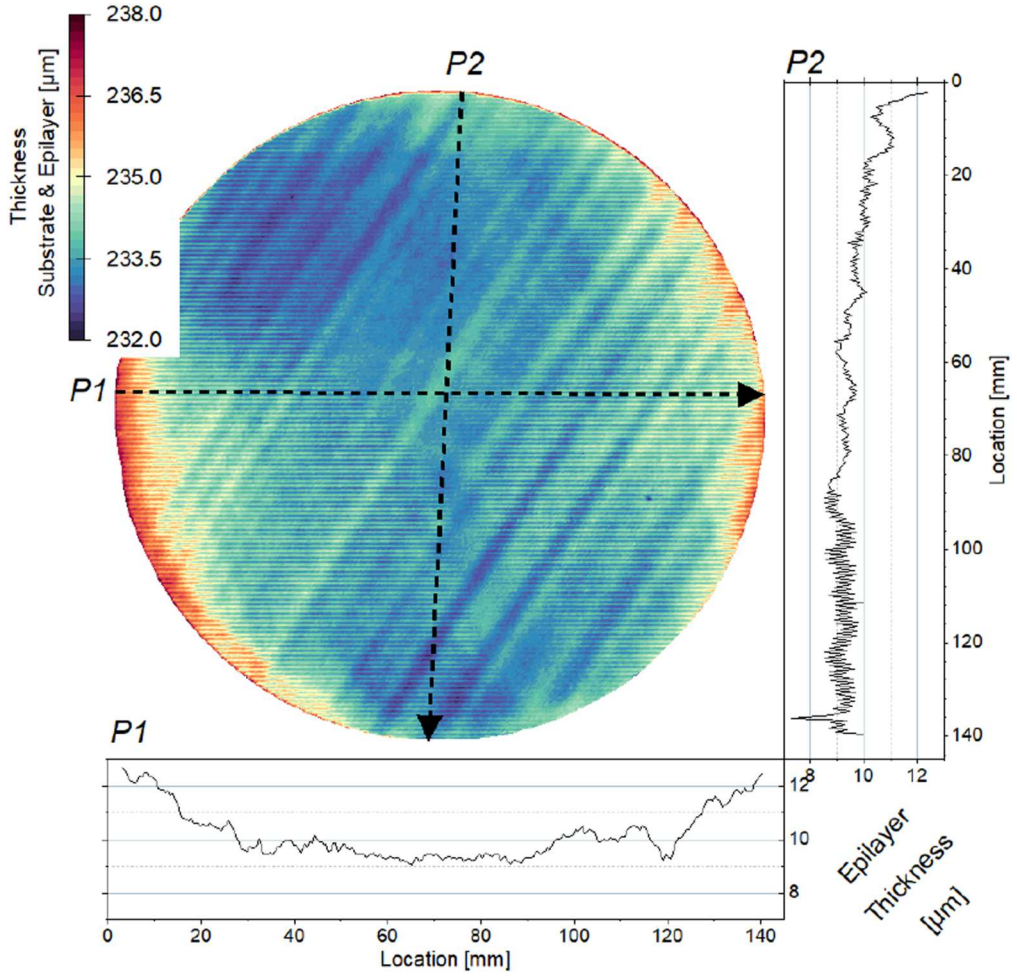

Figure 3. Thickness map of substrate and germanium epilayer of a H_2-med sample shown after epitaxy. The profiles P1 and P2 show the epilayer thickness extracted from thickness maps after subtracting the substrate contribution.

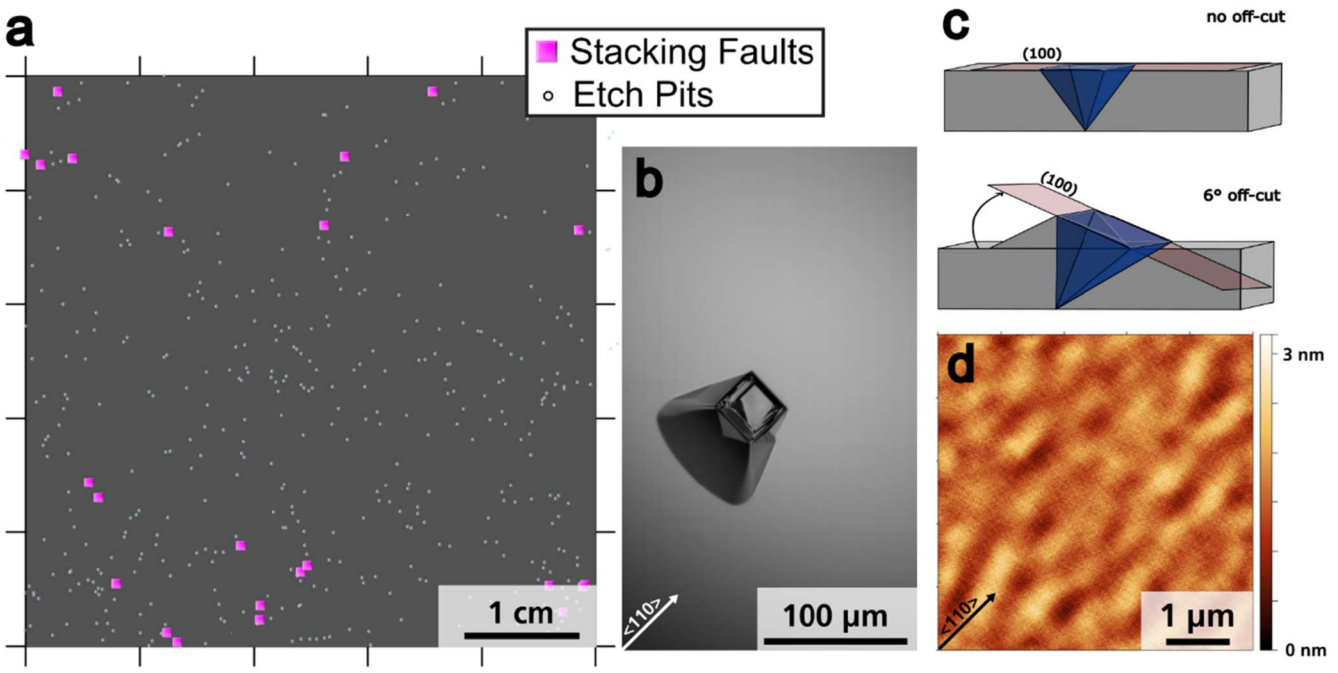

Figure 4. (a) - Defect density map differentiating between clearly classified stacking faults and etch pits. (b) **-** A microscope image in DIC mode of a stacking fault. (c) - A sketch depicting the hill-formation of stacking faults due to offcut. (d) - a 5 × 5µm AFM scan of a wafer from experiment T-med with a RMS-value of 0.2 nm.

across the whole wafer could not be reliably extracted from the thickness maps due to alignment limitations between the pre- and post-epitaxy measurements. Therefore, the average epilayer thickness of 9.3 µm determined by gravimetry for the wafer shown in Fig. 3 is compared to the epilayer thickness, determined from P1 in Fig. 3. In the central region of the wafer (9.7 ± 0.4 µm), they show good agreement.

In the following the quality characterization results of samples from experiment T-med, which achieved the most promising yield and growth rate, are presented. High crystal quality of the epilayers was verified by comparing a rocking curve of the substrate-only to a rocking curve of a substrate with a 10 µm germanium epilayer from experiment T-med. Neither peak broadening nor peak shift is observed, indicating a high crystallinity and additionally proves that there is no change in orientation, hence the 6°-offcut remains. In addition, SPA-LEED measurements showed a sharp diffraction pattern, revealing a p(2 × 2) super cell surface structure and thereby verifying a good surface quality of the epilayer. The data of the rocking curves and the SPA-LEED measurements are not shown in this publication.

The inspection of the wafers under the optical microscope at a magnification of 50x and in differential interference contrast (DIC) mode, a mode which is sensitive to surface topography, the surface appeared mostly smooth and uniform at this scale. The ripple-like structure as seen in the thickness measurements was not visible. However, pyramidal stacking faults (SFs) were detected. Fig. 4b shows a DIC microscope image with an example of a pyramidal SF, while the surrounding area appears featureless. The SF resembles an inverted fourfold pyramid as dictated by the crystallographic orientation of the (100)-surface. Due to the 6°-offcut the SF pyramid is tilted accordingly, and a hill is formed to compensate the difference between the offcut wafer surface and the (100)-plane, accordingly SFs are visible under the optical microscope without DSE as seen in Fig. 4b. This hill-formation at SFs is visualized in Fig. 4c. The SFs are predominantly located near the wafer edges and at contact points, where particles were introduced by sample handling with tweezers during gravimetric weighing and loading into the susceptor under gray room conditions. Eliminating the gravimetric characterization once the optimal process parameters are defined will reduce the handling steps and thereby limit the introduction of particles and other surface defects.

One wafer from the T-med process was analyzed by DSE followed by a manual quantification of etch pits and SFs at the microscope. The resulting defect density map of the analyzed $5 \times 5\,cm^2$ area in the center of the wafer is shown in Fig. 4a. The stacking fault density (SFD) in this area is $0.88\,cm^{-2}$, they are marked as pink squares in the map. No additional SFs were identified in addition to the hill-SFs, which were already visible prior to DSE. All other etch features are marked as blue diamonds in the map and contribute to an etch-pit-density (EPD) of $16.5\,cm^{-2}$. Etch pits are normally classified as delineated threading dislocations, however the classification of the different types of etch features with the used etchant on germanium is not yet fully understood. Thereby all pits and grooves were manually counted, this could include etch artefacts, scratches, stains, microparticles or surface related defects that resemble the shape of pits that are normally attributed to threading dislocations. Accordingly, a definite number for the threading dislocation density (TDD) cannot be stated, but the TDD must be lower than the EPD of $16.5\,cm^{-2}$. Taking both densities into account, the total structural defect density is below $17.4\,cm^{-2}$.

Roughness mappings of $5 \times 5\,\mu m^2$ by the means of AFM of all samples and experiments showed RMS-values below 1 nm, which meets the substrates roughness requirement for subsequent III−V solar cell fabrication. Several measurements at distributed positions of the wafer were done, verifying a homogeneous smoothness over the whole 6 inch wafer area. At process temperatures of 850 °C, epilayers with RMS-values below the detection level of 0.2 nm could be achieved. Comparing the average RMS-values of at least three samples per process parameter, increasing smoothness with increasing process temperature is observed. In experiment T-med, the average RMS-value taking into account AFM-measurements of five wafers is 0.40 nm. The smoothest wafer produced in the experiment T-med, has an RMS value of 0.2 nm. The according roughness mapping is depicted in Fig. 4d. The surface topography

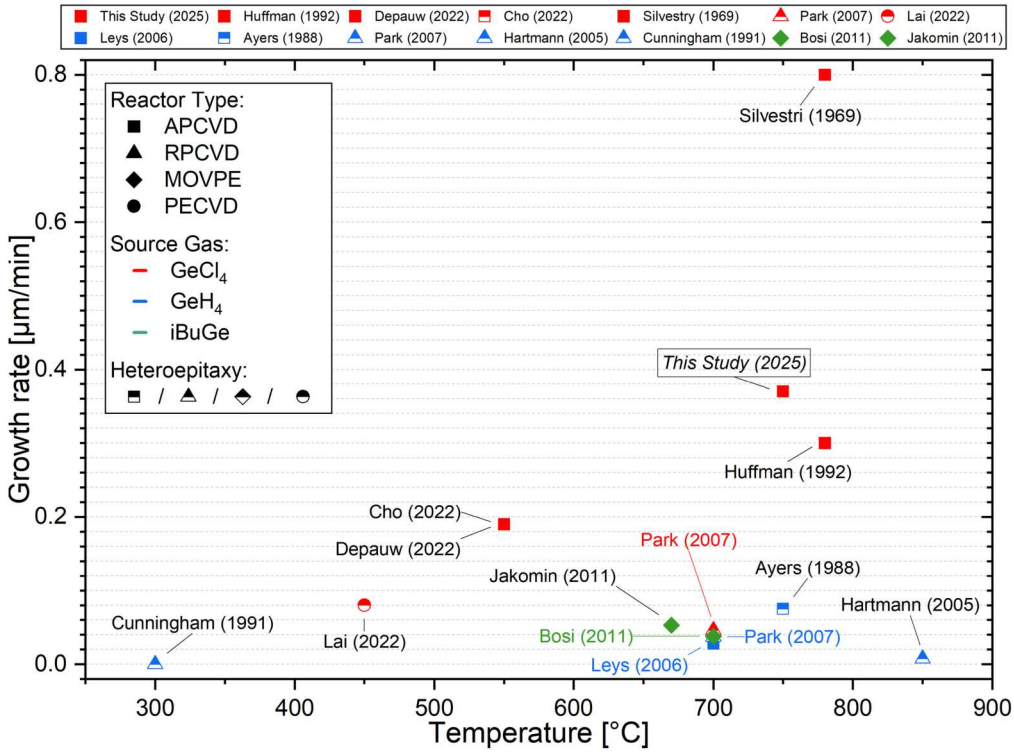

Figure 5. Overview of growth rates from germanium CVD in relation to temperature reported in literature. The shape of the data points represents the type of reactor and the color represents the type of source gas used. Datapoints are only partially filled shapes if the corresponding study was not done on germanium substrates, but on Si or GaAs substrates.

and RMS-values of the epilayers grown in T-med are comparable to epiready substrates reported by Stolle et al.[35] and therefore meet the required RMS-value specification for III−V solar cell processing.

Discussion

To reduce the processing time and increase throughput, a process to produce thick high-quality germanium epilayers of $>10\,\mu m$ was developed, achieving fast growth rates and a high yield in a batch APCVD reactor. First the high growth rates are compared to reported growth rates in literature, then the characterization of the crystallinity of the produced epilayers are evaluated.

In Fig. 5, a selection of germanium CVD growth rates in literature are put into relation with the growth rate achieved in experiment T-med (red square, marked as "This Study") and are discussed in the following. Please note that not all growth rates of epitaxial germanium processes reported in the literature can be included. Particularly, studies that achieve high growth rates and studies representing various process conditions with different source gases, CVD-reactor configurations, and process parameters have been selected for comparison.[9,19–21,26–29,36–39] The influence of source gas partial pressure or ratio is not displayed in Fig. 5, as not all studies reported the exact ratios or not in comparable units. Comparison to the influence of $GeCl_4/H_2$ ratio in this study are discussed and compared to selected studies later in this chapter. Some conclusions on the influences of the differing process parameters could be made by comparing the reported growth rates plotted in Fig. 5. First, the highest reported growth rates are from studies executed in APCVD reactors (squares). Second, using $GeCl_4$ (red) as the source gas, in contrast to GeH_4 (blue) as reported by Park,[28] higher growth rates can be achieved at the same process conditions. As a result, highest growth rates above $0.17\,\mu m\,min^{-1}$ are reported for germanium epitaxy using $GeCl_4$ in an APCVD reactor (red squares).

The growth rate achieved in the present work at the highest $GeCl_4/H_2$-ratio and medium temperature is $0.37\,\mu m\,min^{-1}$ (see Fig. 2), which is higher than $0.30\,\mu m\,min^{-1}$ reported by Huffman et al.[19] for comparable growth parameters in a non-industrial single wafer reactor. Silvestri[17] reported significantly higher growth rates in the range of 0.1 up to $1\,\mu m\,min^{-1}$ for wafer sizes of less than 1 inch, however characterization of the crystallinity solely in the form of surface morphology evaluation at an optical microscope in bright field mode were made. While these findings contributed to the advancement of germanium epitaxy in a $GeCl_4$-H_2 based system, the limited size and standard of both the reactor and substrate wafer as well as the lack of characterization of the crystallinity complicates the comparison to growth rates of more recent studies executed in reactors of microelectronic standard.

In 2022 Cho et al.[21] and Depauw et al.[9] demonstrated a growth rate of up to $0.19\,\mu m\,min^{-1}$ on 8 inch Ge-on-Si[21] as well as on engineered germanium substrates[9] using a single wafer APCVD reactor of microelectronic standard.[9] In both studies, higher $GeCl_4$ mass flows were not explored, suggesting that even higher growth rates may be achievable. The growth rate in this study of $0.37\,\mu m\,min^{-1}$, is almost double of what was reported by Cho[21] and Depauw[9] and could be achieved in a batch type APCVD reactor, producing 14×6 inch wafers simultaneously, resulting in an overall increased throughput in comparison to all other literature listed in Fig. 5.

Process Optimizations and Growth Dynamics

To determine the highest achievable growth rates in the reactor, the influence of process temperature, $GeCl_4/H_2$-ratio and linear gas stream velocity on the deposition rate was evaluated as seen in Fig. 2. Little growth rate dependence on the temperature in the range of 690 to 850 °C can be seen. Calculation of the activation energy of $1.6\,kcal\,mol^{-1}$ from the temperature variation experiments T-low, T-med and T-high confirms a mass-transport- limited regime.[20] In a mass-transport-limited regime the introduction of source-gases plays a driving role in the deposition reaction. The influence of the $GeCl_4/H_2$-ratio needed to be investigated, as it is well established

that hydrogen plays an active role in the deposition reaction of $GeCl_4$, following the Langmuir–Hinshelwood mechanism.[40,41]

According to Ishii et al. $GeCl_{2(g)}$ is formed from $GeCl_{4(g)}$. Then $GeCl_{2(g)}$ and $H_{2(g)}$ are both absorbed on the germanium surface and the subsequent reaction of the absorbed species $GeCl_{2(abs)}$ and $H_{2(abs)}$ leads to deposition of $Ge_{(s)}$ and $HCl_{(g)}$ is released as a byproduct.[42] Thermodynamic equilibrium calculations of the deposition reactions, taking into account all other forming Ge–Cl–H species, predict a decreasing efficiency of the deposition reaction at high Cl/H ratios, as etching by the chloride species is assumed.[42,43] In contradiction to these thermodynamic calculations, an increasing growth rate with increasing $GeCl_4/H_2$-ratio is apparent in Fig. 2. This is in accordance with the ratio dependence reported by Cho et al.[21] and Park et al.,[28] both do not report any etching at higher $GeCl_4/H_2$-ratios.

In the experiments conducted the $GeCl_4/H_2$-ratio was changed by keeping a constant flow of $GeCl_4$-H_2 mix coming from the bubbler and only variating the diluting hydrogen carrier gas flow, whereby a change in the linear gas stream velocity is directly linked to the change in ratio. As mentioned, the large bell volume, requires a high carrier gas flow, and a high gas stream velocity to ensure a homogeneous deposition on all 14 vertically aligned substrates. A decrease in growth rate with increasing linear gas stream velocity can be explained by a "lateral-gas flow limited, mass-transport-limited growth regime" introduced by Silvestri.[20] In this regime the deposition reaction is so rapid, only a fraction of the gas flowing through the reaction chamber is capable of diffusing to the substrate surface for epitaxial deposition. The fraction of gas flowing by unreacted is hereby highly dependent on system geometry and flow conditions.[20] With a molar yield of up to 38%, the experimental data presented is in accordance with the experiments done by Silvestri, where 33% of the gas is involved in the deposition reaction in the linear gas stream limited growth regime at high temperatures.[20]

In contrast to the tube-type-reactor setup used by Silvestri, where the substrate is not rotated and positioned horizontally to the gas stream, in this study the substrates are positioned parallel to the gas flow, on a vertical susceptor, which rotates with 6 rpm. It can therefore be assumed that the gas flow here is not laminar, and that the gas velocity is not constant throughout the total volume of the reaction chamber, but influenced by the geometry of the susceptor and the temperature difference between the "cold"-wall and the hot susceptor. Nevertheless, it cannot be excluded that the gas velocity of the gas introduced into the chamber impacts the growth rate. To separately investigate the $GeCl_4/H_2$-ratio on the growth rate, a constant hydrogen carrier-flow must be set and solely the content of $GeCl_4$ in the $GeCl_4$–H_2 mix coming from the bubbler must be varied.

The upper limit regarding the growth rate has not yet been determined here, indicating potential for further improvement of the process parameters. Higher growth rates could be achieved by either further reducing the hydrogen flow and thereby increasing the $GeCl_4/H_2$-ratio above 1.11×10^{-2}, or by introducing more $GeCl_4$ into the $GeCl_4$-H_2-mix flow by raising the bubbler-temperature. However, further increase of growth rate needs to be cautiously investigated, as there will be a point where a too high growth rate could go together with a loss in epilayer crystal quality. Furthermore, the author assumes a decrease of the hydrogen carrier flow could lead to a larger difference in thickness of top and bottom pocket.

Quality Assessment and Material Characterization

The hydrogen carrier gas flow is known to influence the thickness homogeneity regarding top and bottom pocket in the APCVD reactor used in this study. Previous silicon epitaxy experiments in the same reactor using trichlorosilane ($SiCl_3H$) have shown higher growth rates in the top pocket of the susceptor, whereby an increase of hydrogen carrier gas flow reduced the difference of top and bottom pocket deposition rate, improving the thickness homogeneity over the susceptor area.[11] A directly inverse trend was observed concerning germanium epitaxy in the same reactor; a higher deposition rate on the bottom pocket was achieved in all experiments.

Furthermore, a change in hydrogen carrier gas flow rate did not improve or reduce the thickness inhomogeneity of top and bottom pocket. The contradicting trends of the influence of hydrogen carrier flow on the vertical growth rate inhomogeneity in the reactor used in this study is assumed to be attributable to differing mass transport of the species $GeCl_4$ and $SiCl_3H$. Mass transport can be influenced by various parameters; temperature, gas velocity, diffusivity of species etc. To investigate the exact mechanism a simulation or thorough in situ process analysis would be necessary, this would exceed the scope of this study.

The influence of the presence of Chlorine species on the topography and roughness of the germanium epilayers has been primarily investigated for heteroepitaxial processes on Silicon. It was found that dangling bonds are saturated with Cl during growth, either acting as a morphactant leading to a change in relative surface energy of the different crystallographic planes or by kinetically inhibiting germanium diffusion on the growing surface, whereby the growth of 3D islands is hindered and smooth surfaces can be achieved, even at high temperatures and high growth rates.[25,28,44] Park et al.[28] compared the use of $GeCl_4$ and GeH_4 in heteroepitaxy on Si at identical growth conditions and found that at higher deposition temperature in a $GeCl_4$-H_2 based system in a mass-transport-limited growth regime a smoother surface can be achieved, but for epitaxial deposition from GeH_4 the contrary is the case.[28]

The presented results for $GeCl_4$ showed a comparable trend achieving the smoothest epilayer at a deposition temperature of 850 °C. As mentioned, the highest deposition temperature tested was excluded due to the thermal expansion of up to 1 mm at 850 °C. With an average roughness of 0.4 nm the process at 750 °C and a $GeCl_4/H_2$-ratio of 1.11×10^{-2} produces epilayers which are viable candidates as substrates for III–V epitaxy. Whereas the temperature dependence of the roughness is apparent, no change in roughness was observed for variating $GeCl_4/H_2$-ratios. This is in accordance with reports by Silvestri for experiments in the mass-transport-limited growth regime.

The epilayer-to-epilayer homogeneity of T-med, with an average thickness of 11 μm and a standard deviation of 0.3 μm (2.73%), is acceptable for III–V solar cell fabrication, considering that an absolute wafer-to-wafer thickness variation of ±10 μm is typically tolerated for substrates.[45] Exemplarily on a bottom pocket sample from sample group H_2-med in Fig. 3, it could be shown that the within-wafer homogeneity (including substrate and epilayer) shows a slight improvement in the relative TTV to 2.5% after epitaxy, as locally higher deposition on initially thinner substrate regions, compensated the wedge like thinning of the substrate. Whereas XRD-mapping confirmed that the 6° offcut towards [111], which necessary for a successful III–V nucleation and thus subsequent solar cell processing, remained unaffected. The within-epilayer thickness homogeneity, extracted from the horizontal profile P1 in Fig. 3, revealed an increased deposition toward the wafer edges, which can be attributed to the susceptor design and is consistent with similar observations in silicon homoepitaxy in the same reactor. Given that the wafer edges are not processed into active areas in III–V solar cells, edge-related thickness variations have a smaller impact on device performance, making the homogeneity of the central region of 6 inch wafers most important. The epilayer thickness of 9.7 μm with a standard deviation of ±0.4 μm (4.2% relative variation) extracted from the central region of P1 agrees well with the wafer-average thickness of 9.3 μm determined by gravimetry. Reports on germanium epilayer thickness homogeneity are limited, this complicatesthe assessment of its suitability for III–V solar cell processing. Poortmans et al.[46] reported a 10% uniformity requirement for silicon thin-film solar cells, which is well above the variations observed here. Compared to commercial epiready germanium Cz substrates, the epilayers produced exhibit comparable wafer-to-wafer and within-wafer homogeneity, indicating suitability for subsequent III–V solar cell processing.

With process parameters of T-med smooth germanium epilayers with a uniform average thickness of 11.0 μm and an average

roughness of 0.4 nm could be produced. This is well below the roughness specifications of <1 nm and meets the requirements for substrates used in III−V solar cell fabrication.[1,18,35]

Defect selective etching (DSE), revealed a stacking fault density (SFD) of 0.88 cm^{-2}, and an etch pit density (EPD) of 16.5 cm^{-2}, including all stains, scratches and particles detected resulting in a total defect density below 17.4 cm^2. It is assumed that the main source for SF nucleation are the particles introduced during handling and loading of the substrates in a gray room environment.

Huffman et al.[19] reported "macroscopic" defect densities of germanium homoepitaxial layers below 10 cm^{-2} resulting from particles in the growth chamber, a stacking fault density below 10 cm^{-2} and light haze induced by oxygen contamination. These defect densities were determined by the means of extensive microscopy, no use of defect selective etchant is mentioned. Named authors[19] produced these epilayers at comparable growth conditions as the wafer inspected after DSE in this study. With the SFD being one order of magnitude lower than previously reported for germanium homoepitaxy by Huffman et al.,[19] a higher epilayer quality is indicated. Further research findings on structural defect densities in homoepitaxial germanium layers are scarce.

To further evaluate the structural characterization of germanium epilayers, we compare homoepitaxially deposited silicon epilayers deposited in the same reactor, where SFDs below 1 cm^{-2} and EPDs below 50 cm^{-2} are achieved.[47,48] Here dislocations generated at the wafer edges due to thermal stresses contribute largely to the EPD. These dislocations propagate by slip on the {111}-planes towards the center and are therefore called slip lines.[47,49,50] The detected EPD of 16.5 cm^{-2} in the germanium epilayer is lower than in silicon epitaxy experiments conducted in the same reactor, despite the fact that the critical stress for dislocation generation in germanium is lower, and dislocation mobility is higher than in silicon.[1,49] Both factors would be expected to increase dislocation density and, consequently, the EPD. The SFD of 0.88 cm^{-2} of the germanium epilayer is comparable to the SFD of the silicon epilayer produced in the same reactor. These results demonstrate that, despite potential defect sources such as particle contamination and thermo-mechanical stresses, germanium epilayers with comparably low defect densities can be obtained.

Conclusions

The aim of this study was to develop a high throughput homoepitaxial germanium deposition process in a atmospheric pressure chemical vapor deposition (APCVD) reactor, using $GeCl_4$. The goal was to produce >10 μm thick, smooth germanium epilayers at a high growth rate and yield without compromising crystal quality. This process was successfully developed at a process temperature of 750 °C, with a $GeCl_4/H_2$-ratio of 1.11×10^{-2}, a linear gas stream velocity of 79 cm min^{-1}, achieving a high growth rate of 0.37 μm min^{-1}, and a high molar yield of 36%. The combination of epitaxial deposition at atmospheric pressure and a $GeCl_4$-H_2 based system is effective in achieving these elevated growth rates. An increased $GeCl_4/H_2$-ratio coupled with a decrease in linear gas stream velocity enhances growth rate. Additionally, the growth rate increases with temperature however, the influence is less significant which is typical in the mass-transport-limited growth regime.

The high crystalline quality of the germanium epilayer was confirmed by XRD and by investigation with differential interference contrast microscopy after defect selective etching. Revealing a low stacking fault density of 0.88 cm^{-2} and etch-pit-density of 16.5 cm^{-2}. Additionally, low roughness was detected, with root mean square values as low as 0.4 nm, measured by atomic force microscopy on 5×5 μm^2 areas. Furthermore, good thickness homogeneity was demonstrated, making these epilayers suitable as substrates for III−V solar cell applications. Future efforts will focus on transferring the germanium epitaxy process to engineered virtual substrates, introducing dopants to the epitaxial process, and further confirming quality through solar cell fabrication.

Acknowledgments

The authors thank all involved technicians and scientists at Fraunhofer ISE for executing crucial technical modifications to the reactor, enabling epitaxial deposition of germanium and for their input in many valuable discussions, namely Philipp Häuber and Marion Drießen. Further we thank Mehdi Hortamani, Amir Amini and Philipp Barth for performing the thickness mappings, AFM measurements and defect selective etching, respectively. We would like to thank Umicore Belgium for providing the germanium substrates and the germanium tetrachloride used in the experiments. This work was funded by the Deutsche Forschungsgemeinschaft (DFG, German Research Foundation)—514509471.

ORCID

Ella Susann Supik https://orcid.org/0009-0001-5293-9066

References

1. *Germanium-based technologies: From materials to devices,* C. L. Claeys and E. Simoen (ed.), (Elsevier, Amsterdam) 10, 53 (2007).
2. M. Wong, J. Li, and X. Zeng, *Front. Environ. Sci. Eng.*, **19**, 25 (2025).
3. C. Hernandez, Y. Campidelli, and D. Bensahel, *Process for obtaining a layer of single-crystal germanium on a substrate of single-crystal silicon, and products obtained*, United States, US 6,537,370 B1 (2003).
4. N. Paupy et al., *Nanoscale Adv.*, **518**, 4696 (2023).
5. M. Grohol and C. Veeh, *Study on the critical raw materials for the EU 2023 - Final Report ET-07-23-116-EN-N*, Directorate-General for Internal Market, Industry, Entrepreneurship and SMEs (European Commission) (2023).
6. G. van Hoof, M. Schurmans, B. Robertz, J.-F. Ménard, and K. Dessein, *J. Sustain. Metall.*, **62**, 333 (2020).
7. H.-C. Luan, D. R. Lim, K. K. Lee, K. M. Chen, J. G. Sandland, K. Wada, and L. C. Kimerling, *Appl. Phys. Lett.*, **7519**, 2909 (1999).
8. Y. Bogumilowicz, J. M. Hartmann, C. Di Nardo, P. Holliger, A.-M. Papon, G. Rolland, and T. Billon, *J. Cryst. Growth*, **2902**, 523 (2006).
9. V. Depauw et al., *Prog. Photovolt. Res. Appl.*, **3112**, 1315 (2022).
10. E. Winter, W. Schreiber, P. Schygulla, P. L. Souza, S. Janz, D. Lackner, and J. Ohlmann, *J. Cryst. Growth*, **602**, 126980 (2023).
11. C. Weiss, W. Schreiber, M. Drießen, R. Sorgenfrei, T. Liu, M. Ohnemus, and S. Janz, *37th European Photovoltaic Solar Energy Conference and Exhibition*, ed. N. Pearsall et al. (WIP, Munich, Germany) (2020).
12. J. Cho et al., *IEEE J. Photovoltaics*, **144**, 623 (2024).
13. H. Kum, D. Lee, W. Kong, H. Kim, Y. Park, Y. Kim, Y. Baek, S.-H. Bae, K. Lee, and J. Kim, *Nat. Electron.*, **210**, 439 (2019).
14. J. S. Ward, T. Remo, K. Horowitz, M. Woodhouse, B. Sopori, K. VanSant, and P. Basore, *Prog. Photovolt. Res. Appl.*, **249**, 1284 (2016).
15. A. Chapotot, B. Ilahi, J. Arias-Zapata, T. Hanuš, A. Ayari, G. Hamon, J. Cho, K. Dessein, M. Darnon, and A. Boucherif, *Mater. Sci. Semicond. Process.*, **168**, 107851 (2023).
16. M. K. Hudait, P. Modak, S. Hardikar, K. Rao, and S. B. Krupanidhi, *Materials Science and Engineering: B*, **551-2**, 53 (1998).
17. S. M. Ting and E. A. Fitzgerald, *J. Appl. Phys.*, **875**, 2618 (2000).
18. B. Depuydt, A. Theuwis, and I. Romandic, *Mater. Sci. Semicond. Process.*, **94-5**, 437 (2006).
19. J. E. Huffman and N. L. Casey, *J. Cryst. Growth*, **1293-4**, 525 (1992).
20. V. J. Silvestri, *J. Electrochem. Soc.*, **1161**, 81 (1969).
21. J. Cho, C. Porret, V. Depauw, G. Courtois, D. McDermott, R. Loo, K. Dessein, and R. Kurstjens, *49th Photovoltaics Specialists Conference (PVSC) IEEE*, Philadelphia, PA, USA (2022).
22. R. A. Levy, *Microelectronic Materials and Processes* (Springer Netherlands, Dordrecht) (1989).
23. L. A. Chow, "Equipment and Manufacturability Issues in CVD Processes." *Handbook of Thin Film Deposition*, ed. K. Seshan (William Andrew Publishing, Elsevier, Oxford), 6127 (2012).
24. D. M. Dobkin and M. K. Zuraw, *Principles of Chemical Vapor Deposition* (Springer Netherlands, Dordrecht) (2003).
25. M. Bosi and G. Attolini, *Prog. Cryst. Growth Charact. Mater.*, **563-4**, 146 (2010).
26. F. E. Leys et al., *Thin Solid Films*, **5081-2**, 292 (2006).
27. J. M. Hartmann, A. Abbadie, A. M. Papon, P. Holliger, G. Rolland, T. Billon, J. M. Fédéli, M. Rouvière, L. Vivien, and S. Laval, *J. Appl. Phys.*, **9510**, 5905 (2004).
28. J.-S. Park, M. Curtin, C. Major, S. Bengtson, M. Carroll, and A. Lochtefeld, *Electrochem. Solid-State Lett.*, **1011**, H313 (2007).
29. J.-Y. Lai, S.-C. Tsai, M.-W. Lin, and S. Chen, *Mater. Sci. Semicond. Process.*, **148**, 106740 (2022).
30. U. Scheithauer, G. Meyer, and M. Henzler, *Surf. Sci.*, **1781-3**, 441 (1986).
31. H. SATO, *Method of Evaluating Crystal Defect of Silicon Wafer: Eur. Pat. Appl.*, European Patent Office, EP 1 734 572 A1 (2006).

32. B. O. Kolbesen, J. Mähliß, and D. Possner, *Phys. Status Solidi (a)*, **2083**, 584 (2011).
33. B. Xu et al., *Materials*, **15**, 3594 (2022).
34. R. R. Reeber and K. Wang, *Mater. Chem. Phys.*, **462-3**, 259 (1996).
35. I. Rey-Stolle, E. Barrigón, B. Galiana, and C. Algora, *J. Cryst. Growth*, **31023**, 4803 (2008).
36. J. E. Ayers and S. K. Ghandhi, *J. Cryst. Growth*, **894**, 371 (1988).
37. B. Cunningham, J. O. Chu, and S. Akbar, *Appl. Phys. Lett.*, **5927**, 3574 (1991).
38. M. Bosi et al., *Cryst. Res. Technol.*, **468**, 813 (2011).
39. R. Jakomin, G. Beaudoin, N. Gogneau, B. Lamare, L. Largeau, O. Mauguin, and I. Sagnes, *Thin Solid Films*, **51913**, 4186 (2011).
40. I. Langmuir, *Trans. Faraday Soc.*, **170**, 607 (1922).
41. C. N. Hinshelwood, *Proc. R. Soc. Lond. A*, **113**, 230 (1926).
42. H. Ishii and Y. Takahashi, *J. Electrochem. Soc.*, **1356**, 1539 (1988).
43. V. J. Silvestri, *J. Electrochem. Soc.*, **1196**, 775 (1972).
44. T. I. Kamins, G. A. D. Briggs, and R. S. Williams, *Appl. Phys. Lett.*, **7313**, 1862 (1998).
45. I. Lombardero, M. Ochoa, N. Miyashita, Y. Okada, and C. Algora, *Prog. Photovolt.*, **2811**, 1097 (2020).
46. J. Poortmans, "Epitaxial Thin Film Crystalline Silicon Solar Cells on Low Cost Silicon Carriers." *Thin Film Solar Cells: Fabrication, Characterization and Applications*, ed. J. Poortmans and V. Arkhipov (Wiley, New York), 11 (2006).
47. C. Rittmann et al., *Sol. RRL*, **7**, 78 2200698 (2023).
48. C. Rittmann, E. S. Supik, M. Drießen, F. D. Heinz, Y. P. Botchak Mouafi, F. Schindler, C. Weiss, M. C. Schubert, and S. Janz, *Phys. Status Solidi (a)*, **221**, 2400226 (2024).
49. C. Claeys and E. Simoen, *Extended Defects in Germanium* (Springer Berlin Heidelberg, Berlin, Heidelberg) (2009).
50. *Handbook of Semiconductor Silicon Technology*W. C. O'Mara, R.B. Herring, and L.P. Hunt (ed.), (Noyes Publications, Park Ridge, NJ) (1990).